Porous Anodic Metal Mxides

Zixue Su Wuzong Zhou*

(School of Chemistry, University of St Andrews, St Andrews, Fife KY16 9ST, UK)

Porous anodic aluminium oxide (AAO) and anodic titanium oxide (ATO) attracted an increased attention in the recent years due to their high potentials of application in nanotechnology. This article presents a brief review of some important developments of these smart materials including anodization methods, formation mechanisms of the pores, self-ordering processes and applications. Anodization of other metals are also highlighted.

Key words Anodic aluminium oxide, anodic titanium oxide, nanotechnology, scanning electron microscopy, transmission electron microscopy

1 Introduction

The research realms of fabrication and application of nanomaterials have attracted more scientists and engineering from various disciplines in the recent years. Nanomaterials often have novel properties, many of which are yet to be investigated. On the other hand, our knowledge of nanoscale chemical processes for these materials is also very limited. One example is formation of nanoporous anodic metal oxides.

Anodic metal oxides have diverse applications in prevention of corrosion of metal substrates from their service environment[1], forming capacitor dielectrics[2,3], templating nanomaterials[4-9] and in many other fields such as catalysis, optics and electronics[10-13]. The best known porous anodic oxide, anodic aluminium oxide (AAO), was first reported 50 years ago[14-17] and is now commercially available because its pores can be used as template for preparing various nanoparticles, nanowires and nanotubes. Porous anodic oxide films have also been achieved on surfaces of many other metals, sometimes the so-called valve metals, e. g titanium[18-20], hafnium[21] niobium[22], tantalum[23], tungsten[24], vanadium[25], and zirconium[26].

It has been widely accepted that the formation of the pores in anodic metal oxides is based on two continuous processes, one is oxide dissolution at the electrolyte/oxide interface and the other is oxidation of metal at the oxide/metal interface. In fact, the formation mechanism of these pores, often hexaganolly ordered, is much more complicated than people normally predicted. Although the formation mechanism, pore ordering, pore size control have been extensively studied[27-29] and many efforts have been made to optimize the anodization conditions for these films[30-32], there is still much work to do in order to fully understand the electrochemical process during the anodization.

This article presents a brief review of the research progress in fabrication, application and understanding the formation mechanism of anodic metal oxides, especially the AAO and anodic titanium oxide (ATO).

2 Anodic aluminium oxide

Anodization is an electrochemical process which could create a thick compact oxide layer on surface of a metal substrate. This type of non-porous surface coating layer can normally increase the resistances to corrosion and wear of metals. Therefore, this technique has been applied to many metals, e. g. aluminum, magnesium, niobium, tantalum, titanium, tungsten, vanadium, zinc, and zirconium, etc. Among them, AAO films are most commonly used to protect aluminum alloys.

In a typical anodizing process, an aluminium metal foil is connected to the anode of a dc power supply. A weak acidic solution is normally used as electrolyte. The cathode can be made by any conducting material which is unreactive in the electrolyte. Once the external voltage is switched on, hydrogen ions are reduced to produce hydrogen gas at cathode

and aluminium is oxidized into Al^{3+} cations. Part of the cations are dissolved into electrolyte and part of them form an oxide layer on the metal surface. For the latter reaction, oxygen-containing anions are supplied by the electrolyte.

Depending on the electrolyte used, two types of anodic aluminium oxide layers could be produced: nonporous barrier oxide layers with uniform thickness in a near neutral electrolyte and porous anodic oxide films containing dense nanoscale pores in an acidic or alkaline electrolyte[33,34].

2.1 Chemical reactions

Chemical reactions during the anodization of aluminium look simple. For example, the overall reaction can be written as $2Al + 3H_2O \rightarrow Al_2O_3 + 3H_2$[31]. This reaction is correct, but does not reflect the the details of the whole electrochemical process. It is essential to understand the chemical reactions at electrolyte/oxide and oxide/metal interfaces separately. It is certain that, when electric field is supplied, aluminium at the oxide/metal interface will be oxidized into Al^{3+} cations: $Al \rightarrow Al^{3+} + 3e$. Some of these cations migrate across the oxide layer and are dissolved into the electrolyte (in a case of porous AAO) or form oxide at the electrolyte/oxide interface (in a case of nonporous AAO). Some of them stay at the oxide/metal interface, forming Al_2O_3 with the oxide anions migrated from the electrolyte/oxide interface. There is still an unsolved problem regarding the above reactions, i. e. the form of the oxygen-containing anions is uncertain, which could be O^{2-} or OH^-. At least in anodization of titanium, it has been recently found that the wall of ATO nanotubes contains two layers with the outer layer of titanium hydroxide, implying that some anions must be OH^-[35]. The hydroxide will eventually decompose to form oxide. In the case of AAO, even hydroxide of aluminium forms as an intermediate phase, it will decompose very quickly and no detectable hydroxide layer appears.

At the electrolyte/oxide interface, Al_2O_3 is dissolved in electrolyte. The oxide anions are driven by the electric field to move crossing the oxide layer, contributing to the formation of Al_2O_3 at the oxide/metal interface. However, these oxide anions are not enough for the newly formed oxide layer. A significant amount of anions must be supplied from dissociation of water at the electrolyte/oxide interface. A water-splitting reaction: $H_2O \rightarrow 2H^+ + O^{2-}$ or $H_2O \rightarrow H^+ + OH^-$ was therefore proposed[36,37].

It was recently reported that dissociation of water not only supplies anions to the oxide layer, but also plays an important role in governing the porosity of the porous AAO films and the overall reaction at the electrolyte/oxide interface can be written as:

$$Al_2O_3 + nH_2O \rightarrow 2Al^{3+} + (3 + n - x)O^{2-} + xOH^- + (2n - x)H^+ \quad (1)$$

where n is introduced to indicate the ratio of the dissociation rate of water to the dissolution rate of Al_2O_3 and x indicates the ratio of O^{2-} and OH^-, which has not yet been determined[38].

In addition to the above principal reactions, some anions in electrolyte may also be incorporated in the aluminium oxide layer. For example, an oxide film grown in phosphoric acid electrolyte may contain phosphorus species, probably as PO_4^{3-} anions[39,40]. These large anions migrate much slower than O^{2-} / OH^- anions and are unlikely able to approach to the oxide/metal interface[41]. Therefore, water in electrolyte is still the main source of oxygen for the formation of the oxide films[42].

2.2 Nonporous barrier layer

The history of anodization of aluminum dates back to the beginning of the last century. Protection and decoration of Al and its alloys by means of an anodic treatment was developed as early as in 1920's[1]. In fact, even without anodization, aluminum metal could react with air, forming a thin barrier oxide layer with a thickness of 2—3 nm on the surface[43]. This compact barrier oxide layer protects the surface from further oxidization by its service environment and is an excellent electrical insulator. When an aluminum foil with a native oxide coating is used as an anode in an electrolytic cell, the electrical potential across the oxide layer can be increased without initiating current flow until the field in the oxide layer is high enough to drive aluminum and oxide ions through the oxide layer[44,45]. The ionic transport across the oxide layer under a high field plays an important role in oxide formation during the anodization of aluminum[42]. Electric field strength in a range from 10^6 to 10^7 V/cm is sufficient to drive the ions crossing the oxide layer. It has been generally accepted that during the formation of nonporous anodic alumina in a near neutral electrolyte, e. g. an ammonium tartrate or ammonium pentaborate solu-

tion, aluminium oxide simultaneously grows at both electrolyte/oxide and oxide/metal interfaces. Oxygen-containing anions, O^{2-}/OH mainly coming from dissociation of water at the electrolyte/oxide interface move inwards to react with aluminum at the oxide/metal interface to form oxide. At the same time, Al^{3+} cations move outwards from the metal surface to react with water at the electrolyte/oxide interface to form oxide. It has been established that the total ionic current density (j) under a high field conduction relates with the electric field strength (E) through an exponential law $j = j_0 \exp(\beta E)$ where j_0 and β are temperature-dependent constants involving parameters of ionic transport in a particular material[14,15].

It was reported that, when aluminium was anodized in a sodium borate-ethylene glycol electrolyte, the fraction of the total charge carried by cations (tAl^{3+}) was about 0.6, whereas in aqueous ammonium citrate tAl^{3+} varied from 0.37 to 0.72 as the current density increased from 0.1 to 10 mA/cm^2[16]. Some other values of the transport numbers of Al^{3+} cations were also detected[47-49].

As the oxide is insoluble in a near neutral electrolyte, a barrier layer forms at near 100% efficiency, i.e. almost all of the Al^{3+} cations migrating from the oxide/metal interface would contribute to the formation of Al_2O_3 at the electrolyte/oxide interface[50]. Brown et al. gave a ratio of oxide formation at oxide/electrolyte and oxide/metal interfaces to be 40% : 60%. Such films grow by counter migrations of Al^{3+} and O^{2-} ions, with the latter accounting for about 60% of the ionic current[51]. The final thickness of the barrier oxide is proportional with the applied voltage, and has a small deviation with temperature and the electrolyte characteristics. A typical anodization ratio for aluminum anodized in a near neutral electrolyte is about 1.4 nm/V[33,52].

According to the newly established equifield strength model[35], in a near-neutral solution when dissolution of Al_2O_3 can be neglected, the thickness of the oxide layer (d) will continuously increase if the field assisted anionic migration carries on. This process will not stop until d approaches a critical value, d_C, when the corresponding electric field strength, $E_C = U/d_C$, is merely too weak to drive the anions crossing the oxide barrier layer. Finally, a uniform thickness (d_C) and constant electric field strength (E_C) will be approached in the whole area of the barrier layer. Consequently, the morphology of the oxide/metal interface will replicate that of the electrolyte/oxide interface as shown by a scanning electron microscopic (SEM) image in Fig. 1 presented by Furneaux et al.[53]. A schematic diagram for the equifield strength model of a nonporous AAO is shown in Fig. 2A, in which, the field at any point across the oxide layer, e.g. A′A, B′B or C′C, has a constant strength.

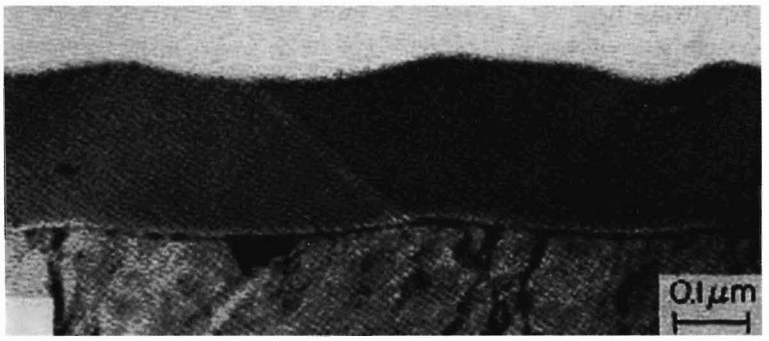

Fig. 1 SEM image of a cross section of an amorphous aluminium oxide layer (top) grown on aluminium (bottom) in 0.16 M ammonium tartrate at 20℃ with a current density of 10 mA/cm^2, voltage of 200 V. The oxide thickness is about 220 nm, equivalent to 1.1 nm/V[53]

2.3 Pore formation in porous AAO films

In the recent years, much attention has been paid to porous AAO films rather than the nonporous barrier oxide layer because they have applications in nanoscience and nanotechnology. Although AAO with highly dense pores was first reported in 1950's[11], AAO films with highly ordered pores were obtained 40 years later[30].

When aluminum is anodized in an acidic solu-

tion, due to the relatively high solubility of alumina in the electrolyte, the thickness of the oxide layer can never approach to the critical value, d_C. Both the dissolution process of oxide and oxidation process of aluminium can carry on without stop. In a stead state, a new balanced thickness of oxide layer, d_B, will be achieved corresponding to field strength of E_B, where d_B is smaller than d_C and E_B is greater than E_C.

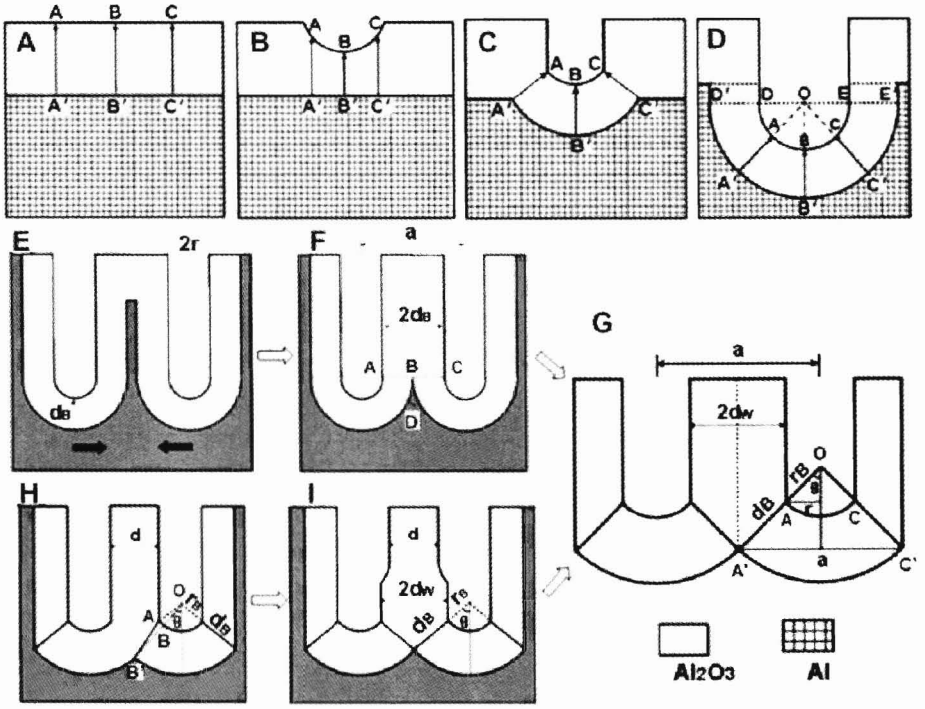

Fig. 2 Schematic diagrams for the electric-field strength distribution in some typical oxide barrier layers with the electrolyte/oxide interface marked by A, B, C and the oxide/metal interface marked by A′, B′, C′. (A) Planar oxide layer with a uniform thickness. (B) Planar layer with a corrosive pit. (C) The surface of a corrosive pit at the electrolyte/oxide interface is replicated at the oxide/metal interface. (D) Formation of the hemispherical pore base and a cylindrical wall of a single pore. (E) Two pores have a separation larger than $2d_B$. (F) The pores move towards each other to achieve a wall thickness of $2d_B$. (G) The pores move closer with a balanced curvature of $2\theta < 180°$. (H) Two pores are too close to each other and (I) their self-adjustment to increase the wall thickness[35]

The initiation and growth of pores are associated with accelerated dissolution of aluminium oxide with an influence of electric field[27]. More detailed investigations[15,29] suggested that electropolishing or other pretreatment could leave a slightly scalloped surface of aluminum covered by an oxide coating layer.

It is believed that, a large number of defects such as impurities, dislocation, grain boundaries, or nonmetallic inclusions in the underlying metal could cause a faster dissolution rate and lead to a pit growth[54,55]. It has been also reported that, when Al^{3+} cations are ejected from the oxide surface driven by an applied field, cation vacancies can arise and accumulate to form high density voids in the oxide layer, which can help the propagation of pits[56,57]. Therefore, an applied electric field can increase the pit number and growth rate rapidly, which has been supported by Hebert and co-workers in their studies of anodic etching and pitting corrosion of aluminum[58,59]. According to the equifield strength model, a pit site has a relatively thinner oxide layer, leading to a faster oxidation rate[38]. For example, the field strength at B′B is higher than that at A′A or C′C in Fig. 2B. Pores are eventually developed on these pits.

The cell and pore diameter were generally considered to be proportional to the applied voltage[14,15,60,61]. By assuming a hemispherical pore bottom, Parkhutik and Shershulsky[61] established a theoretical model and found that the cell size, R_m, is a linear function of the applied potential U_0. $R_m = 2.5$ nm/V was calculated for a mild anodization case

where the electric field strength across the barrier is about 0.77 V/nm[60].

According to the equifield strength model, the pore growth direction should be perpendicular to the surface of the oxide layer. In the case of a rough surface, the pores may not be parallel to each other as being often observed experimentally. Furthermore, a single pore tends to increase its size since both the oxide layer thicknesses and the field strength at the pore bottom and the pore wall are the same (Fig. 2D). In practice, the increase of the pore size is limited by the neighbouring pores. Further investigation indicated that the pore size is determined by the relative dissociation rate of water, since the thickness of the oxide layer is fixed with the certain anodization conditions and the wall thickness is also determined (Fig. 2G)[38]. It is interesting that other conditions influence the pore size via the relative dissociation rate of water. From Fig. 2D, one can see that hemispherical pore bottom is the only morphology which can meet the requirement of the equifield strength model.

2.4 Mechanism of pore ordering

When suitable anodization voltage and electrolyte are used, hexagonal ordered pores can be easily produced in AAO films (Fig. 3a). It has also been found from experiments that the ordering can be improved with increasing the anodization time. Perfect hexagonal anodic alumina pores array with a very narrow size distribution and extremely high aspect ratios over an area of a micrometer scale was grown by Masuda et al. via a two-step anodization process using a 0.3 M oxalic acid solution under a constant voltage of 40 V at 0℃[30,62]. In the first step, Al foil was anodized for more than 10 h, then the produced AAO film was wet etched away by the so-called P-C etch at 80℃ using a mixture of 35 ml/l 85% H_3PO_4 and 20 g/l CrO_3. The second step was re-anodization of the aluminium foil with a periodic surface roughness. The nanopore array formed in the second step exhibited excellent regularity. Soon after that, they successfully obtained a perfect hexagonal patterned anodic alumina films with an area as large as of 2 mm × 2 mm by a nanoprinting method[63]. A hexagonally patterned SiC surface created by electron beam lithography was used to "nanoprint" the Al surface prior to anodization, leading to a highly ordered AAO array. Besides, Bandyopadhyay et al.[64] found that hexagonally ordering could also be obtained via a high current density electropolishing process. These reports confirmed that a patterned pore array can guild the pore growth.

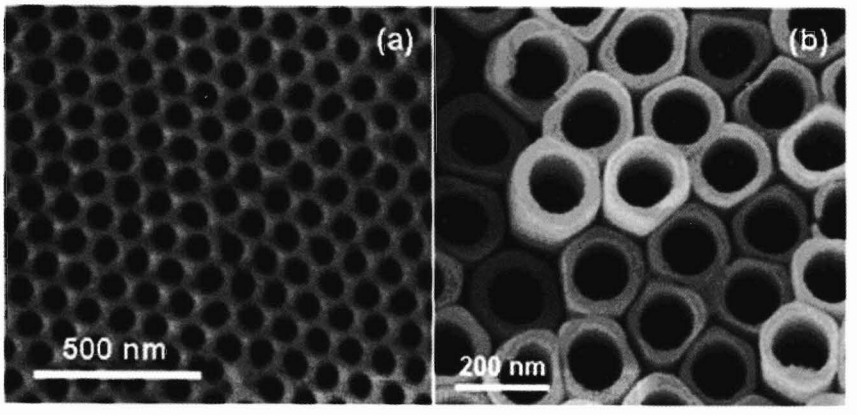

Fig. 3 Typical top-view SEM images of (a) AAO and (b) ATO films. The AAO film was prepared by two-step anodization: an aluminum plate was anodized in 0.3 M oxalic acid at 40 V for 3 h, the porous oxide layer was removed by a mixed solution of chromic and phosphoric acid, and the plate was anodized again for 10 h. The ATO film was prepared with the anodizing voltage of 60 V for 16 h[35]

Singh et al.[65] attributed the pore initiation and self organization of the porous structures in aluminum oxide films at the initial stage to the significant elastic stress in the oxide layer. The main element of this theory is the Butler-Volmer relation[66] describing an exponential dependence of the current on the overpotential and a dependence of the activation energies of the oxide-electrolyte interfacial reactions on the Laplace pressure and the elastic stress in the oxide layer. In the case when the

effect of elastic stress is negligible, a weakly nonlinear analysis leads to formation of spatially irregular pore arrays that have been observed in experiments. In the case when the effect of elastic stress in the oxide layer is significant, the instability can transform from a long-wave type to a short-wave type. A weakly nonlinear analysis of the short-wave instability shows that it leads to the growth of spatially regular, hexagonally ordered pore arrays.

Vorobyova et al. [67] considered distribution of an applied voltage in three main components of an electrochemical bath system: a growing oxide layer; a Helmholtz layer at electrolyte/oxide interface; and a Gouy-Chapman space charge layer, which extends to the quasi-neutral electrolyte region. It is found that the transformation of the Helmholtz layer is due to self-organization effects in the Gouy-Chapman layer, leading to a growth of highly ordered pores.

Although the principle of the pore ordering has been investigated extensively[15,17,30,35,65 69], the most commonly accepted model is based on mechanical stress during the oxidation process[17,70]. The ionic density of Al^{3+} in anodic alumina (3.66×10^{22}/cm^3) corresponding to the weight density of approximately 3.1 g/cm^3[71] is significantly lower than the atomic density of aluminum metal of 6.02×10^{22}/cm^3. The mechanical stress coming from volume expansion during oxide formation at the oxide/metal interface could be a possible origin of a repulsive force between neighboring pores. Jessensky et al. [17] proposed that this repulsive force should be accounted for the self-organized formation of hexagonal pore arrays. It was also suggested that neither too large nor too small expansion would result in a long range ordering of the pores. Only a medium volume expansion of 1.2 times from aluminum to alumina, independent of the specific anodization conditions, could lead to an ordering[72].

On the other hand, the recently established equifield strength model gave a new explanation for the pore ordering[35,38]. When a single pore grows to form a cylindrical wall as shown in Fig. 2D, the field strength along DD′ or EE′ in the wall of the pore is the same as that at the pore bottom, the oxide layer can move not only downwards but also sidewards. In other words, a single pore may continuously increase its pore diameter, although this development is restricted by a high pore density and fixed porosity under certain anodization conditions.

When two pores are quite separated as shown in Fig. 2E, they will expand and, therefore, the neighboring walls will move towards each other until two walls merge with a thickness of the combined wall, $2d_B$ (Fig. 2F). When two pores are too close, i.e., where $d<2d_W$, the pores will move apart to increase the wall thickness as demonstrated in Fig. 2H and 2I, in order to meet the requirement of the equifield strength. Since the final pore size and porosity are determined by the anodization conditions (discussed below), these processes lead to a movement of pores, i.e. self-adjustment. When such self-adjustment of the pore-pore distance takes place two dimensionally in the whole area, a hexagonal pattern can be achieved.

2.5 Porosity and water dissociation

It has been experimentally observed that the cell dimension and pore diameter of AAO films change significantly with the applied voltage[14,15,60,61]. For example, measured from large-area hexagonal pore arrays, an interpore distance (D_{int}) = 63 nm when sulphuric acid (H_2SO_4) was used as electrolyte and working voltage was 25 V[72,73], D_{int} = 100 nm when oxalic acid ($H_2C_2O_4$) was used as electrolyte and voltage was 40 V[30,73], D_{int} = 90 − 140 nm with an aged sulphuric acid solution, a high anodization potential up to 70 V and a high current density up to 200 mA/cm^2[74], D_{int} = 220 − 300 nm with oxalic acid at 110 − 150 V[60], D_{int} = 500 nm when applying phosphoric acid (H_3PO_4) and 195 V[73,75].

On the other hand, the porosity of AAO films seems to be insensitive with the applied voltage. Nielsch et al. [73] proposed a 10% porosity rule based on measurement on the produced AAO films under various experimental conditions. They found self-ordered porous AAO required a porosity of 10%, independent of the specific anodization conditions. This empirical model was not in agreement with some other reports[76,77] and was challenged by a more recent work from the same group, in which a much smaller porosity, 3.3%, was detected[60].

The nature of the voltage-dependent porosity of AAO is not fully understood. A recent report revealed that the key factor to influence the porosity (P) is the relative rate of water dissociation (n) on the oxide surface, where n is defined by equation (1), with a very simple relation of $P=3/(n+3)$

(Fig. 4)[35,38]. Increasing the voltage can enhance the water dissociation greater than oxide dissolution and therefore reduce the porosity. From Fig. 4, one can find that the so-called 10% porosity rule has no special physical meaning. This value was often observed probably because the normal anodization conditions give a relative water dissociation rate of about 27.

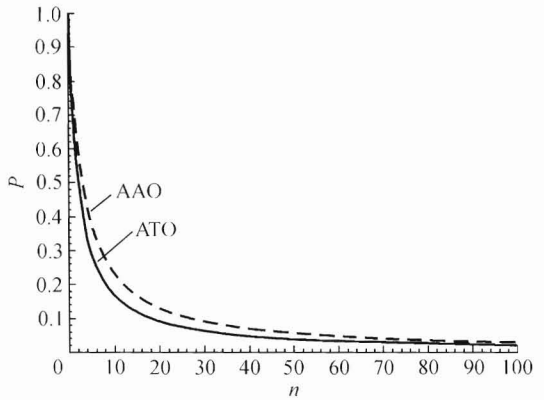

Fig. 4 Porosities (P) of AAO and ATO as functions of the relative dissociation rates of water (n) at the electrolyte/oxide interface

From the same model, similar exponential relations between the porosity and voltage (U) has also be derived as

$$P = 213\exp\left(-6.46\frac{U}{d_{\text{final}}(1-\exp(-\gamma U))+d_0}\right) \quad (2)$$

where d_0 describes the thickness of the native oxide layer when no voltage is applied, d_{final} is a measure of the maximum thickness, and γ stands for the increase of the thickness with U.

Relations between the porosity and other anodization parameters, such as current density, field strength can also be established. The simulated results can match the experimental data very well[38].

The simple relation between the porosity of anodic oxide films and the relative water dissociation rate needs to be further confirmed with more experimental data. The relative dissociation rate of water cannot be directly detected, nor does the dissolution rate of alumina. A theoretic study of the field assisted water dissociation rate, i. e. a calculation of dissociation energy of water as a function of field strength, will be interesting.

3 Anodic titanium oxide

The most significant difference between typical anodic titanium oxide (ATO) and anodic aluminum oxide (AAO) is that the latter is a continuous film with a pore array while the former consists of separated nanotubes as demonstrated in Fig. 3. Several recent studies have showed that titania nanotubes have better properties compared to many other forms of titania for applications in photocatalysis[78,79], gas sensors[80-83], photoelectrolysis[12,84,85], and photovoltaics[13,86-88]. Since Zwilling et al. reported the anodization of titanium in chromic acid and hydro fluoride acid for the first time in 1999[89], great achievements have been made in the fabrication, characterization, application and formation mechanism of ATO materials[90].

3.1 Selection of electrolytes and chemical reactions

So far, several different electrolytes have been used for producing ATO. Gong, et al. reported their ATO preparation in a 0.5 wt% HF aqueous solution at room temperature using different anodizing voltages, from 3 to 20 V[18]. Fig. 5 shows SEM images of a typical ATO sample. Appearance of separated nanotubes became obvious when the voltage is high.

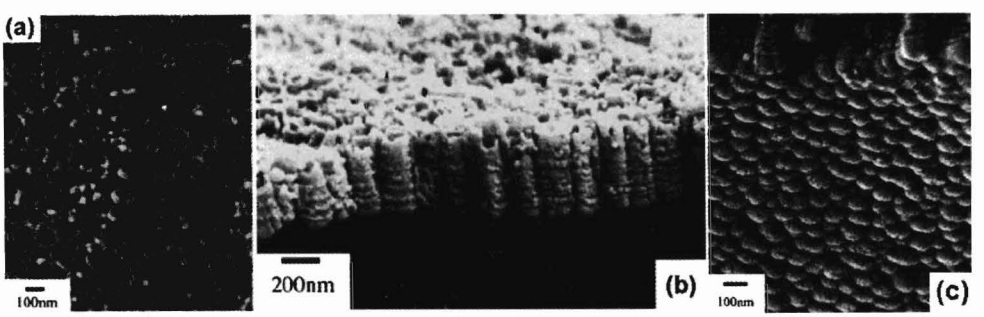

Fig. 5 FE-SEM top view (a), cross sectional (b), and bottom view images of titanium oxide nanotubes anodized in 0.5 wt% HF solution at 20 V for 20 min. (from Ref[18])

It was noticed that the film thickness could not be increased further from 400—500 nm using HF-based electrolyte. Fluoride solution can help to dissolve TiO_2 by forming $[TiF_6]^{2-}$ anions. However, too strong acidity of HF-solution results in a too fast dissolution of the formed TiO_2 nanotubes. Mixture with other acids did not help very much, but the quality of the nanotube arrays could be varied. Mor et al. reported that addition of acetic acid to a 0.5 wt% HF electrolyte in a 1∶7 ratio resulted in more mechanically robust nanotubes without changing their shape and size[81,91]. Ruan, et al. found that the surface morphology of nanotube arrays anodized in an electrolyte containing 2.5% HNO_3 and 1% HF at 20 V for 4 h showed a uniform, clean, regular nanotube structure with a length about 400 nm, while an electrolyte of 0.5M H_3BO_3-2.5% HNO_3-1% HF in anodization at 20 V for 4 h led to a greater degree of pore irregularity, with a nanotube length about 560 nm[92].

When using a KF or NaF solution as an electrolyte, thickness of ATO films can be significantly increased[93]. The acidity of the electrolyte might be tuned by adding HF, H_2SO_4 or Na_2SO_4 in order to adjust the balance of dissociation of titania at the electrolyte/oxide interface and oxidation of titanium at the oxide/metal interface[94,95]. The better electrolyte is probably a NH_4F-based solution. From a mixed solution of NH_4SO_4 and NH_4F, the ATO film can grow up to several micrometers in thickness[19].

Considering diffusion as the main effect on local acidification[19], which could lead to a temporarily increased dissolution rate, Macak et al. used glycerol solutions as electrolytes with very low diffusion constant to suppress a pH burst at the pore tip which, they believed, led to the growth of ridges on the sidewall of anodic TiO_2 nanotubes (seen clearly in Fig. 5b). They demonstrated an ATO sample prepared in a glycerol electrolyte with 0.5 wt% NH_4F with a length of 7 μm and a high degree of regularity and homogeneity as shown in Fig. 6[32].

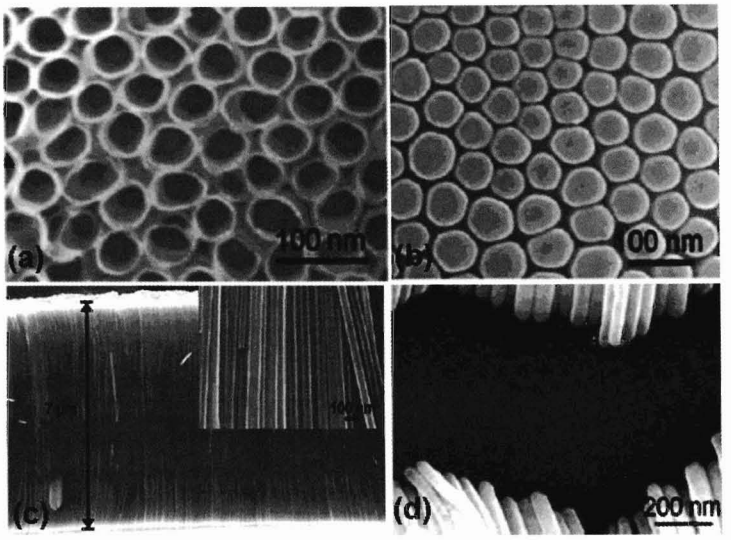

Fig. 6 SEM images of smooth ATO with a length of 7 μm produced in a glycerol electrolyte with 0.5 wt% NH_4F: (a) top view; (b) bottom view; (c) cross sectional view. The inset of (c) shows the walls of the nanotubes in more details. (d) Top view of an anodized sample after removal of some arrays of nanotubes. (from Ref[32])

In combination with either HF, KF, or NaF to provide fluoride ions, Grimes and co-workers[20,96] obtained nanotube arrays up to approximately 220 μm in length using a variety of organic electrolytes including dimethyl sulfoxide (DMSO), formamide (FA), ethylene glycol, and N-methylformamide (NMF) (Fig. 7). It was suggested that, the key to successfully achieving very long nanotube arrays was to minimize water content in the anodization bath to less than 5%. As with or-

ganic electrolytes, donation of oxygen is more difficult in comparison with water, thus reducing the tendency to form oxide[97] and slowing down the process of the nanotube growth. At the same time, the reduction in the water content reduces the chemical dissolution of the oxide in the fluorine containing electrolytes and hence aids the longer-nanotube formation.

It is widely accepted that the key processes responsible for the formation of ATO should be the same as that of AAO[90]: (1) oxide growth at the surface of the metal occurs due to an interaction of titanium with O^{2-} or OH^- anions[12]; (2) Ti^{4+} cations migrate from the oxide/metal interface to the electrolyte/oxide interface and are ejected into solution by an electric field; (3) field assisted dissolution of the oxide at the electrolyte/oxide interface[15].

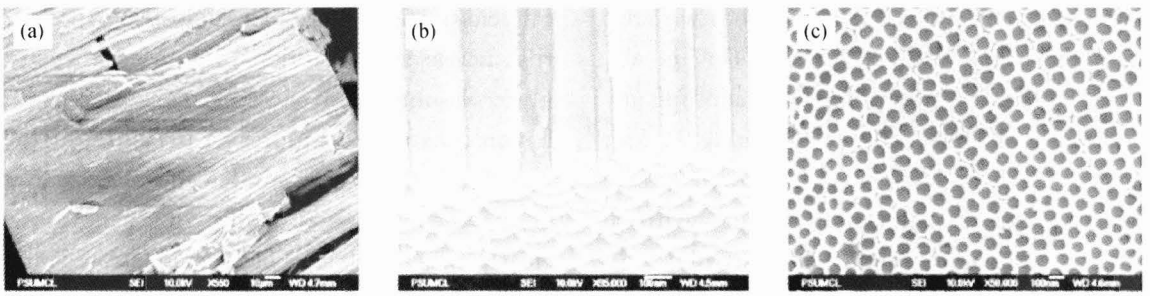

Fig. 7 FESEM cross-sectional (a), bottom (b), and top (c) images of an ATO grown at 60 V in an ethylene glycol electrolyte containing 0.25 wt% NH_4F (from Ref[96])

The above processes cannot explain the formation of the gaps between the titania nanotubes. When individual nanotubes were examined by using TEM, it was found that the wall of the nanotubes consists of two layers. The inner layer was titania and the outer layer was titanium hydroxide (see the next section), implying that OH^- anions can move from the electrolyte/oxide interface to the oxide/metal interface to form a titanium hydroxide layer, although the exact formula could not be determined. It was assumed that the hydroxide layer decomposed continuously into oxide during the anodization since its thickness at the nanotube bottom maintains constant. Consequently, the principal chemical reaction at the hydroxide/metal interface should be: $Ti + xOH^- \rightarrow Ti(OH)x + 4e^-$ and titanium hydroxide decomposes to form TiO_2 at the oxide/hydroxide interface. The overall reaction at the electrolyte/oxide interface was proposed to be:[35]

$$TiO_2 + nH_2O + F^- \rightarrow [TiF_6]^{2-} + O^{2-} + OH^- + H^+ \quad (3)$$

where n was introduced for the same reason as in the case of AAO. Like AAO, water dissociation and OH^- ionic migration should not be ignored.

3.2 Formation of nanotubes and porosity

The formation mechanism of the pores in the ATO nanotubes should be similar to that of AAO, i.e. the pores are developed from pits on the foil surface and continue their growth based on a balance of the dissolution of oxide at the electrolyte/oxide interface and oxidation of titanium metal at the oxide/metal interface[90]. The equifield strength model[35] can explain the morphology of the hemispherical nanotube bottom and the often observed distortion of the pore shape as shown by the top-view SEM images (Fig. 5—7), because the pores have an tendency to increase their sizes.

However, some researchers have different opinions. Macak et al. suggested that oxide dissolution in the growth of ATO was a dominant factor rather than the electric field aided ion transportation. As the dissolution rate of titanium oxide greatly depend on the local acidity in a F-containing electrolyte, the pores grow at the higher acidic pore bottom rather than the low acidic pore mouth[19,32,98]. This model cannot explain the regular shape and ordering of the pores at an early stage. It is even more difficult to elucidate the formation of the gap between the nanotubes using this model.

The argument about the formation of the gap

between the nanotubes did not approach to an end when the detailed structure of the ATO nanotubes were not be revealed. Mor et al. proposed that the metallic part between the pores underwent oxidation and field assisted dissolution[90]. So far no experimental support for this model was found.

Since the discovery of a double layer wall of ATO nanotubes (Fig. 8A), the understanding of the gap formation in ATO became much easier. Originally, there is no gap between the nanotubes. Instead, a hydroxide layer forms in between the nanotubes as shown in Fig. 8D. Because the density of this layer is lower than that of titania, when it decomposes into titania, a volume contraction takes place. If the contraction direction is perpendicular to the wall, the nanotubes are separated (Fig. 8E). If the contraction direction is parallel to the wall, ridges on the surface of the nanotubes form a series of O-rings with a constant distance (Fig. 8B and 8F). HRTEM images confirmed that these O-rings contained β-form titania (Fig. 8C). This elucidation is different from a current transient model gaven by Macak et al.[32]. In the latter, it was believed that relatively regular current oscillations occur during anodization. It was found that when the frequency of the current oscillations was converted into a length scale, it compared well to the distance between ridges on the side walls of the nanotubes. Thus, the current transients are correlated with the variations in the wall thickness. This can be explained by the fact that every current transient is accompanied by a pH burst at the pore tip. It seems to be true that further investigation including more detailed studies of these ridges will be carried out to reveal their formation mechanism.

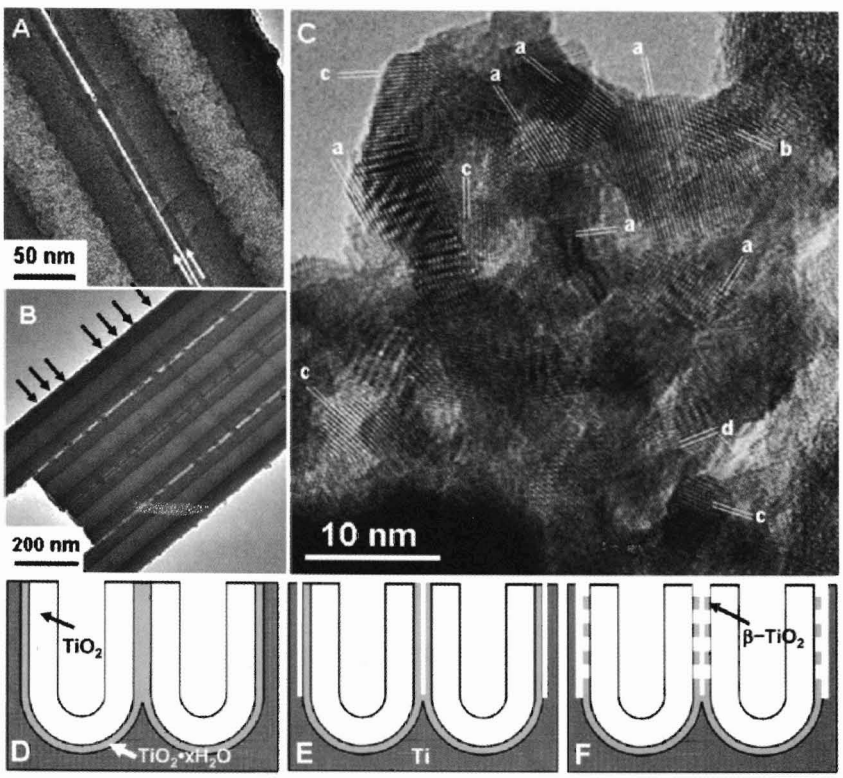

Fig. 8 TEM images of (A) the lower part of ATO nanotubes, showing outer layers of titanium hydroxide indicated by two arrows, and (B) the upper part of ATO nanotubes, which decompose into clusters of titania nanocrystallites. (C) HRTEM image of a typical cluster. (D)—(F) show the formation of a titanium hydroxide outer layer (D), its partial dehydration into two separated layers (E) and its further dehydration into clusters of titania nanocrystallites (F)[35]

Similar to AAO, a large amount of O^{2-}/OH anions are needed to build the wall of nanotubes and these anions are mainly from dissociation of water. Therefore, even using an organic electrolyte, a few percentage of water must be added. The relation of the porosity (P) and the relative dissociation rate of

water for ATO is also simple, $P=2/(n+2)$ derived from equation (3) (Fig. 4) (Supporting Information of[35]). In the calculation, the difference of densities of titania and titanium hydroxide was ignored and the authors only laid their account with the porosity of the pores without including the gaps between the nanotubes. In addition, it was assumed that all the oxide anions from dissolution of titania migrated to the other side of the oxide layer and contributed to the formation of oxide. While in experiments, oxygen bubbles are often observed on the anode. Therefore, more accurate calculation is still needed in future work.

4 Other anodic metal oxides

To date, there are a number of other metals have been tried to produce porous oxide films. The anodizaing ratio varies from 1.60 nm/V to 2.20 nm/V[33].

Anodization of hafnium. Hafnium oxide has many interesting properties, e.g. its high chemical and thermal stabilities, high refractive index and relatively high dielectric constant[99,100]. These properties make hafnium oxide a valuable material to be used as a protective coating, optical coating, gas sensor or capacitor[101-105]. Self-organized porous hafnium oxide layers were obtained successfully for the first time by Tsuchiya and Schmuki[21] via anodization of hafnium at about 50 V in 1 M H_2SO_4 + 0.2 wt% NaF at room temperature. Anodization potential was found to be a key factor affecting the morphology and the structure of the porous oxide. The pore diameter was found to increase with increasing potential. Porous hafnium oxide layers with high aspect ratios can be grown to a thickness of several tens micrometers.

Anodization of niobium. Porous niobium oxide structures could be applied in gas sensors[106], catalysis[107], and optical[108] and electrochromic[109] devices. Anodization of niobium has been studied in various electrolytes[110,111]. Self-organized porous anodic niobium oxide films were successfully obtained by Sieber[22] and Karlinsey[112] in 1 M H_2SO_4 + 1 wt% HF and 1.5% HF respectively. More recently Choi[113] obtained anodic Nb_2O_5 films with an effective thickness over 500 nm, consisting of a protective outer layer of around 90—130 nm and an inner layer of 300—400 nm, via an optimized anodization-annealing-anodization process. Besides, a stress determined formation mechanism was proposed in anodization of niobium by Zhao et al.[111]. Since the volume of niobium pentoxide is much larger than that of the niobium metal, oxidation of niobium metal yields an increase of inner stress in the oxide layer. As the inner stress increases, niobium oxide swells to form bulges and facilitates the oxidation of niobium metal under beneath, leading to formation of microcones. If no bulges generates, strong enough inner stress would break the oxide layer, also leading to growth of microcones.

Anodization of tantalum. Ta_2O_5 has attracted intensive attention due to its application in optical devices, and as a protective coating material for chemical equipment, or suitable material for storage capacitors[115-119]. Anodization of tantalum has been widely investigated in sulfuric, phosphoric acid, and Na_2SO_4 solutions, and a layer of amorphous Ta_2O_5 with a uniform thickness could be obtained[111,120]. Self-organized porous anodic tantalum oxide with a reasonably narrow size distribution was fabricated by Sieber et al.[23,121] via anodizing tantalum in 1 M H_2SO_4 + 2 wt % HF for 2 h after a potential ramp from the open-circuit potential to 20 V with a sweep rate 100 mV/s.

Anodization of tungsten. Tungsten oxide (WO_3) has been receiving considerable attention in recent years for its use in gas sensing[122,123], electrochromic[124-130] and photochromic[131,134] processes, etc. Based on early research in nonporous anodic tungsten oxide films[135-137], nanoporous anodic tungsten oxide was obtained by galvanostatic anodization in oxalic acid by Mukherjee et al., although the regularity of the pores appeared to be rather poor[24]. Since then several groups have made a good progress to some extent in controlling the morphology and ordering of the anodic tungsten oxide[138-140]. For example, de Tacconi et al reported that porous anodic WO_3 made in 0.3 M oxalic acid for 1 h at 35 V showed dense pores with a small pore size distribution[140].

Anodization of vanadium. Glacial acetic acid

with small percentages of water and sodium tetraborate has been found to be the most suitable electrolyte for anodization of vanadium[141 143]. Due to the existence of the unfilled d shell, the phase composition of the anodic vanadium oxide could be rather complicated, such as V_2O_5[144 147], VO_2[141,148,149], or a mixture of V_2O_5 and other oxide phases with lower oxidation states[147,150 152].

Anodization of zirconium. Zirconium oxide is an important functional material that plays a key role as an industrial catalyst and catalyst support[153,154]. It was reported that a compact anodic zieconium oxide layer of up to several hundred nanometers in thickness can be achieved in many electrolytes[155]. A unique feature in comparison with other anodic metal oxides mentioned above is that the growth of the compact ZrO_2 layer at room temperature directly leads to a crystalline film[156] rather than an amorphous film as observed from other anodic metal oxides. Formation of self-organized porous zirconium oxide layers produced by anodization of Zr at 30 V in an electrolyte of 1M H_2SO_4 + 0.2 wt% NH_4F was reported by Tsuchiya et al.[26,157].

It is noted from the reports about porous anodic metal oxides mentioned in this section that no double layer was detected. The structures are similar to AAO rather than ATO. Perfectly ordered pores for these anodic transition metal oxides have not been achieved yet. In future research for these materials, it is important to refine the anodization conditions to control the dissolution rate of oxides and oxidation rate of the metals.

5 Applications of AAO and ATO

Non-porous anodic alumina films have been widely applied in prevention and decoration of aluminum surface[1], sealing[158 162], dyeing[163 165], and capacitors[2,166]. In the recent years, self-organized porous AAO with perfect hexagonal pore patterns have been used to fabricate a variety of nanomaterials, such as nanoparticles, nanowires and nanotubes[4 9,167,168 171]. The corresponding synthetic methods can be categorized as follows[167]: etching semiconductor substrate using a porous alumina film as a mask[4 6], pattern transfer by replica of porous alumina as a template[30], deposition of functional materials in the form of porous alumina arrays by electroplating and sol-gel[172 174], and deposition of functional materials by chemical vapor deposition (CVD)[7,8,175 177]. As one example, Fig. 9 shows a typical fabrication process of a carbon nanotube array by using a highly ordered AAO film as a template by Li et al.[7].

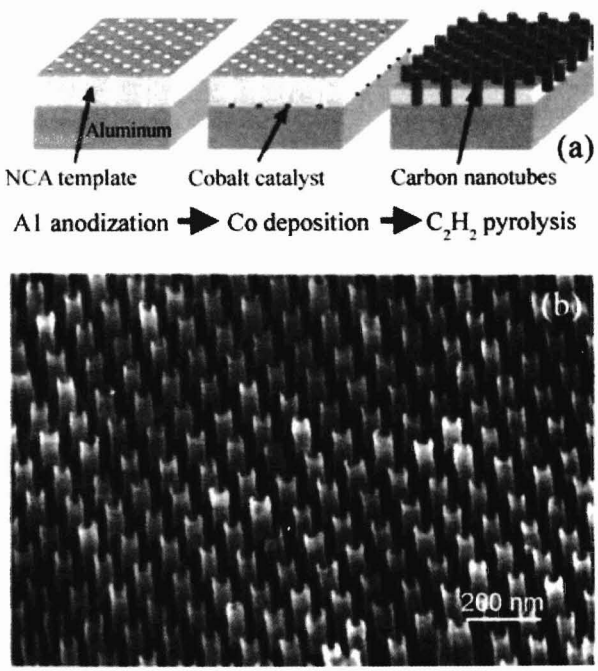

Fig. 9 *(a) Schematic of fabrication process of hexagonally ordered array of carbon nanotubes and (b) the corresponding SEM image of the product (From Ref[7])*

Anodic titania nanotubes could be applied in various fields such as in photoelectrochemical and water photolysis, hydrogen sensing, self-cleaning sensors, and application in heterojunction dye-sensitized solar cells as reviewed by Mor et al[90].

Paulose et al. showed that a crystalline 45 μm long anodic titania nanotube-arrays under UV illumination exhibited a remarkable water photoelectrolysis photoconversion efficiency of 16.25%[20]. A light to electricity photoconversion efficiency of 6.9% was achieved by Shankar et al.[96] using very long nanotube arrays up to 220 μm in backside illuminated dye-sensitized solar cells under AM 1.5 illumination.

Varghese et al.[178] and Paulose et al.[83] reported a transcutaneous hydrogen gas sensor of unprecedented sensitivity as a diagnostic tool for determining lactose intolerance due to lactase deficiency. This hydrogen gas sensor, based on the use of highly-ordered titania nanotube arrays made by anodization of a 250 μm thick titanium foil, shows a remarkable change in electrical resistance of 8.7 orders of magnitude when cycled between air and nitrogen containing 1000 ppm of hydrogen. As hydrogen sensors, the anodic TiO_2 nanotube arrays possess excellent photocatalytic properties with an ability of self-cleaning from contamination with exposure to ambient UV light[91].

It is certain that more applications will be found in the near future. To achieve this, full crystallization of the ATO films will be essential since crystallized titania nanotubes have better conductivity and mechanical strength, while the large surface areas are still maintained. It can be expected that the hydroxide layer in the as-synthesized ATO will help in crystallization, i.e. crystallization would start in the outer hydroxide layer and expand to the inner oxide layer if a reasonably low temperature is carefully chosen and long crystallization time is applied.

In summary, the formation mechanisms of porous AAO and ATO nanotubes have been investigated extensively. For the latter material, the discovery of double layer wall structure is crucial in understanding the appearance of separated nanotubes. With the better knowledge of mechanisms, the fabrication of these anodic oxide films becomes much more controlable. The hydroxide layer and surface ridges in ATO may be useful in improving the quality of the ATO films. As mentioned in the present review, there are still many unsolved problems, e.g. refinement of the anodization conditions, confirmation of the formation mechanism, theoretical study and more accurate calculation of the water dissociation on oxide surface under a electric field, control of the pore size and porosity, full crystallization of ATO films and discovery of more applications of the porous anodic metal oxides, etc. This field will continously attract researchers in future.

Acknowledgements

WZ thanks EPSRC and EaStChem for financial support.

References

[1] Bengough GD, Stuart JM. Brit. Patent 223994, 1923.

[2] Jason AC, Wood JL. Some electrical effects of the adsorption of water vapour by anodized aluminium. Proc Phys Soc B 1955; 68(12): 1105-16.

[3] Dell'Oka CJ, Pulfrey DL, Young L. Physics of thin films. Vol. 6, Ed Francombe MH, Hoffman RW (New York: Academic) 1971, 1-79.

[4] Nakao M, Oku S, Tamamura T, et al. GaAs and InP nanohole arrays fabricated by reactive beam etching using highly ordered alumina membrane. Jpn J Appl Phys 1999; 38(2B): 1052-5.

[5] Liang J, Chik H, Yun A, et al. Two-dimensional lateral superlattices of nanostructures: nonlithographic formation by anodic membrane template. J Appl Phys 2002; 91(4): 2544-6.

[6] Chen L, Yin AJ, Im JS, et al. Fabrication of 50-100 nm patterned InGaN blue light emitting heterostructures. Phys Stat Sol A 2001; 188(1): 135-8.

[7] Li J, Papadopoulos C, Xu JM. Highly-ordered carbon nanotube arrays for electronics applications. Appl Phys Lett 1999; 75(3): 367-9.

[8] Li J, Papadopoulos C, Xu J. Growing Y-junction carbon nanotubes. Nature 1999; 402(6759): 253-4.

[9] Hu W, Gong D, Chen Z, et al. Growth of well-aligned carbon nanotube arrays on silicon substrates using porous alumina film as a nanotemplate. Appl Phys Lett 2001; 79(19): 3083-5.

[10] Basu S, Chatterjee S, Saha M, et al. Study of electrical characteristics of porous alumina sensors for detection of low moisture in gases. Sens and Actuat B: Chemical 2001; 79 (2): 182—6.

[11] Yang BC, Uchida M, Kim HM, et al. Preparation of bioactive titanium metal via anodic oxidation treatment. Biomaterials 2004; 25(6): 1003—10.

[12] Mor GK, Shankar K, Paulose M, et al. Enhanced photocleavage of water using titania nanotube arrays. Nano Lett 2005; 5(1): 191—5.

[13] Mor G. K, Shankar K, Paulose M, et al. Use of highly-ordered TiO_2 nanotube arrays in dye-sensitized solar cells. Nano Lett 2006; 6(2): 215—8.

[14] Keller F, Hunter MS, Robinson DL. Structural features of oxide coatings on aluminum. J Electrochem Soc 1953; 100 (9): 411—9.

[15] O'Sullivan JP, Wood GC. The morphology and mechanism of formation of porous anodic films on aluminum. Proc R Soc Lond A 1970; 317(1531): 511—43.

[16] Thompson GE, Furneaux RC, Wood GC, et al. Nucleation and growth of porous anodic films on aluminum. Nature 1978; 272(5652): 433—5.

[17] Jessensky O, Müller F, Gösele U. Self organized formation of hexagonal pore arrays in anodic alumina. Appl Phys Lett 1998; 72(10): 1173 5.

[18] Gong DW, Grimes CA, Varghese OK, et al. Titanium oxide nanotube arrays prepared by anodic oxidation. J Mater Res 2001; 16(12): 3331 4.

[19] Macak JM, Tsuchiya H, Schmuki P. High-aspect-ratio TiO_2 nanotubes by anodization of titanium. Angew Chem Int Ed 2005; 44(14): 2100—2.

[20] Paulose M, Shankar K, Yoriya S, et al. Anodic growth of highly ordered TiO_2 nanotube arrays to 134 μm in length. J Phys Chem B 2006; 110(33): 16179—84.

[21] Tsuchiya H, Schmuki P. Self-organized high aspect ratio porous hafnium oxide prepared by electrochemical anodization. Electrochem Commun 2005; 7(1): 49—52.

[22] Sieber I, Hildebrand H, Friedrich A, et al. Formation of self-organized niobium porous oxide on niobium. Electrochem Commun 2005; 7(1): 97—100.

[23] Sieber I, Kannan B, Schmuki P. Self-assembled porous tantalum oxide prepared in H_2SO_4/HF electrolytes. Electrochem Solid-State Lett 2005; 8(3): J10—2.

[24] Mukherjee N, Paulose M, Varghese OK, et al. Fabrication of nanoporous tungsten oxide by galvanostatic anodization. J Mater Res 2003; 18(10): 2296—9.

[25] Stefanovich GB, Pergament AL, Velichko AA, et al. Anodic oxidation of vanadium and properties of vanadium oxide films. J Phys: Condens Matter 2004; 16(23): 4013—24.

[26] Tsuchiya H, Macak JM, Sieber I, et al. Self-organized high-aspect-ratio nanoporous zirconium oxides prepared by electrochemical anodization. Small 2005; 1(7): 722—5.

[27] Hoar TP, Mott NF. A mechanism for the formation of porous anodic oxide films on aluminium. J Phys Chem Solids 1959; 9(2): 97—9.

[28] Heber KV. Studies on porous Al_2O_3 growth—I. Physical model. Electrochim Acta 1978; 23(2): 127—33.

[29] Thompson GE, Wood GC. Anodic films on aluminium. In treatise on materials science and technology, Vol. 23: Corrosion: Aqueous Process and Passive Films; Scully, J. C., Ed.; Academic Press Inc.: New York, 1983; Chapter 5, 205—329.

[30] Masuda H, Fukuda K. Ordered metal nanohole arrays made by a two-step replication of honeycomb structures of anodic alumina. Science 1995; 268(9): 1466—8.

[31] Masuda H, Yosuya M, Ishida M. Spatially selective metal deposition into a pore-array structure of anodic porous alumina using a microelectrode. Jpn J Appl Phys 1998; 37(9A/B): 1090—2.

[32] Macak JM, Tsuchiya H, Taveira L, et al. Smooth anodic TiO_2 nanotubes. Angew Chem Int Ed 2005; 44 (45): 7463—5.

[33] Diggle JW, Downie TC, Goulding CW. Anodic oxide films on aluminum. Chem Rev 1969; 69(3): 365—405.

[34] Li FY, Zhang L, Metzger RM. On the growth of highly ordered pores in anodized aluminum oxide. Chem Mater 1998; 10(9): 2470—80.

[35] Su ZX, Zhou WZ. Formation mechanism of porous anodic aluminium and titanium oxides. Adv Mater 2008; 20(19): 3663—7.

[36] Despic A, Parkhutik VP. Electrochemistry of aluminum in aqueous solutions and physics of its anodic oxide. In: Bokris JO, White RE, Conway BE. Modern aspects of electrochemistry. Vol. 23, Plenum Press: New York, 1989, 401—504.

[37] Valand T, Heusler KE. Reactions at the oxide-electrolyte interface of anodic oxide films on aluminum. J Electroanal Chem 1983; 149(1—2): 71—82.

[38] Su ZX, Hahner G, Zhou WZ. Investigation of the pore formation in anodic aluminium oxide. J Mater Chem 2008; 18 (47): 5787—95.

[39] Plumb RC. Studies of the anodic behaviour of aluminium. II. Coulometry of barrier layer production. J Electrochem Soc 1958; 105(9): 498—502.

[40] Dorsey, Jr. GA. The characterization of anodic aluminas. 1. Composition of films from acid electrolytes. J Electrochem Soc 1966; 113(2): 169—72.

[41] Thompson GE, Wood GC. Porous anodic film formation on aluminium. Nature 1981; 290(5803): 230—2.

[42] Siejka J, Ortega C. An O^{18} study of field-assisted pore formation in compact anodic oxide films on aluminum. J Electrochem Soc 1977; 124(6): 883—91.

[43] Sheasby PG., Pinner R. The surface treatment and finishing of aluminum and its alloys, Vol. 1, 6th Ed. Materials Park, Ohio & Stevenage, UK: ASM International & Finishing Publications, 2001, 5.

[44] Guntherschulze A, Betz H. Z Phys Neue Untersuchungen über die elektrolytische Ventilwirkung I. Die Oxydschicht des Tantals. 1931; 68(3—4): 145—61.

[45] Guntherschulze A, Betz H. Die bewegung der ionengitter von isolatoren bei extremen elektrischenfeldstarken. Z Phys 1934; 92(5—6): 367—74.

[46] Davies JA, Domeij B, Pringle JPS, et al. The migration of metal and oxygen during anodic film formation. J Electrochem Soc 1965; 112(7): 675—80.

[47] Xu Y, Thompson GE, Wood GC. Mechanism of anodic film formation on aluminium. Trans Inst Met Finish 1985; 63(3—4): 98—103.

[48] Shimizu K, Kobayashi K, Thompson GE, et al. Development of porous anodic films on aluminium. Philos Mag A 1992; 66(4): 643—52.

[49] Skeldon P, Thompson GE, Garcia-Vergara SJ, et al. A tracer study of porous anodic alumina. Electrochem Solid-State Lett 2006; 9(11): B47—51.

[50] Thompson GE, Xu Y, Skeldon P, et al. Anodic oxidation of aluminium. Philos. Mag. B 1987; 55(6): 651—67.

[51] Brown F, Mackintosh WD. The use of Rutherford backscattering to study the behaviour of ion-implanted atoms during anodic oxidation of aluminium: Ar, Kr, Xe, K, Rb, Cs, Cl, Br, and I. J Electrochem Soc 1973; 120(8): 1096—102.

[52] Hass G. On the preparation of hard oxide films with precisely controlled thickness on evaporated aluminum mirrors. J Opt Soc Amer 1949; 39(7): 532—9.

[53] Furneaux RC, Thompson GE, Wood GC. The application of ultramicrotomy to the electronoptical study of surface films on aluminium. Corros Sci 1978; 18(10): 853—81.

[54] Hebert KR, Wu HQ, Gessmann T, et al. Positron annihilation spectroscopy study of interfacial defects formed by dissolution of aluminum in aqueous sodium hydroxide. J Electrochem Soc 2001; 148(2): B92—100.

[55] Huang RC, Hebert KR, Gessmann T, et al. Effect of impurities on interfacial void formation in aluminum. J Electrochem Soc 2004; 151(4): B227—32.

[56] Chao CY, Lin LF, Macdonald DD. A point defect model for anodic passive films. J Electrochem Soc 1981; 128(6): 1187—94.

[57] Lin LF, Chao CY, Macdonald DD. A point defect model for anodic passive films. J Electrochem Soc 1981; 128(6): 1194—8.

[58] Martin T, Hebert KR. Atomic force microscopy study of anodic etching of aluminum: etching morphology development and caustic pretreatment. J Electrochem Soc 2001; 148(2): B101—9.

[59] Wiersma BJ, Hebert KR. Observations of the early stages of the pitting corrosion of aluminum. J Electrochem Soc 1991; 138(1): 48—54.

[60] Lee W, Ji R, Gösele U, et al. Fast fabrication of long-range ordered porous alumina membranes by hard anodization. Nat Mater 2006; 5(9): 741—9.

[61] Parkhutik VP, Shershulsky VI. Theoretical modeling of porous oxide growth on aluminum. J Phys D: Appl Phys 1992; 25(8): 1258—63.

[62] Masuda H, Satoh M. Formation of gold nanodot array using anodic porous aluminum as an evaporation mask. Jpn J Appl Phys 1996; 35(1B): L126—9.

[63] Masuda H, Yamada H, Satoh M, et al. Highly ordered nanochannel-array architecture in anodic alumina. Appl Phys Lett 1997; 71(19): 2770—2.

[64] Bandyopadhyay S, Miller AE, Chang HC, et al. Electrochemically assembled quasi-periodic quantum dot arrays. Nanotech 1996; 7(4): 360—71.

[65] Singh GK, Golovin AA, Aranson IS. Formation of self-organized nanoscale porous structures in anodic aluminum oxide. Phys Rev B 2006; 73(20): 205422.

[66] Bockris JO, Reddy AKN. Modern electrochemistry (Plenum Press, New York), 1970, Vol. 2.

[67] Vorobyova AI, Outkina EA, Khodin AA. Self-organized growth mechanism for porous aluminum anodic oxide. Russian Microelectronics, 2007; 36(6): 384—91.

[68] Despic AR, Parkhutik VP. Modern aspects of electrochemistry. Vol. 20, Ed: Bockris JO et al (New York: Plenum) 1989, 397.

[69] Yuzhakov VV, Chang HC, Miller AE. Pattern formation during electropolishing. Phys Rev B 1997; 56(19): 12608—24.

[70] Garcia-Vergara SJ, Iglesias-Rubianes L, Blanco-Pinzon CE, et al. Mechanical instability and pore generation in anodic alumina. Proc R Soc A 2006; 462(2072): 2345—58.

[71] Skeldon P, Shimizu K, Thompson GE, et al. Barrier-type anodic films on aluminium in aqueous borate solutions: I. Film density and stopping power of anodic alumina for alpha particles. Surf Interface Anal 1983; 5(6): 247—51.

[72] Li AP, Muller F, Birner A, et al. Hexagonal pore arrays with a 50—420 nm interpore distance formed by self-organization in anodic alumina. J Appl Phys 1998; 84(11): 6023—6.

[73] Nielsch K, Choi J, Schwirn K, et al. Self-ordering regimes of porous alumina: the 10% porosity rule. Nano Lett 2002; 2(7): 677—80.

[74] Chu SZ, Wada K, Inoue S, et al. Fabrication of ideally ordered nanoporous alumina films and integrated alumina nanotubular arrays by high-field anodization. Adv Mater 2005; 17(17): 2115—9.

[75] Masuda H, Yada K, Osaka A. Self-ordering of cell configuration of anodic porous alumina with large-size pores in phosphoric acid solution. Jpn J Appl Phys 1998; 37(11A): L1340—2.

[76] Ono S, Saito M, Ishiguro M, et al. Controlling factor of self-ordering of anodic porous alumina. J Electrochem Soc 2004; 151(8): B473—8.

[77] Ono S, Saito M, Asoh H. Self-ordering of anodic porous alumina induced by local current concentration: Burning. Electrochem Solid-State Lett 2004; 7(7): B21—4.

[78] Adachi M, Murata Y, Harada M, et al. Formation of titania nanotubes with high photo-catalytic activity. Chem Lett 2000; 29(8): 942－3.

[79] Chu SZ, Inoue S, Wada K, et al. Highly porous (TiO_2-SiO_2-TeO_2)/Al_2O_3/TiO_2 composite nanostructures on glass with enhanced photocatalysis fabricated by anodization and sol-gel process. J Phys Chem B 2003; 107(27): 6586—9.

[80] Varghese OK, Gong D, Paulose M, et al. Extreme changes in the electrical resistance of titania nanotubes with hydrogen exposure. Adv Mater 2003; 15(7—8): 624－7.

[81] Mor GK, Carvalho MA, Varghese OK, et al. A room-temperature TiO_2-nanotube hydrogen sensor able to self-clean photoactively from environmental contamination. J Mater Res 2004; 19(2): 628－34.

[82] Varghese OK, Mor GK, Grimes CA, et al. A titania nanotube-array room-temperature sensor for selective detection of hydrogen at low concentrations. J Nanosci Nanotech 2004; 4(7): 733－7.

[83] Paulose M, Varghese OK, Mor GK, et al. Unprecedented ultra-high hydrogen gas sensitivity in undoped titania nanotubes. Nanotech 2006; 17(2): 398－402.

[84] Mor GK, Shankar K, Varghese OK, et al. Photoelectrochemical properties of titania nanotubes. J Mater Res 2004; 19(10): 2989—96.

[85] Varghese OK, Paulose M, Shankar K, et al. Water-photolysis properties of micron-length highly-ordered titania nanotube-arrays. J Nanosci Nanotech 2005; 5(7): 1158－65.

[86] Uchida S, Chiba R, Tomiha M, et al. Application of titania nanotubes to a dye-sensitized Solar cell. Electrochem 2002; 70(6): 418－20.

[87] Adachi M, Murata Y, Okada I, et al. Formation of titania nanotubes and applications for dye-sensitized solar cells. J Electrochem Soc 2003; 150(8): G488－93.

[88] Paulose M, Shankar K, Varghese OK, et al. Backside illuminated dye-sensitized solar cells based on titania nanotube array electrodes. Nanotech 2006; 17(5): 1446－8.

[89] Zwilling V, Aucouturier M, Darque-Ceretti E. Anodic oxidation of titanium and TA6V alloy in chromic media. An electrochemical approach. Electrochim. Acta 1999; 45(6): 921－9.

[90] Mor GK, Varghese OK, Paulose M, et al. A review on highly ordered, vertically oriented TiO_2 nanotube arrays: Fabrication, material properties, and solar energy applications. Sol Energy Mater Sol Cells 2006; 90(14): 2011—75.

[91] Mor GK, Varghese OK, Paulose M, et al. A self-cleaning, room-temperature titania-nanotube hydrogen gas sensor. Sensor Lett 2003; 1(1): 42－6.

[92] Ruan C, Paulose M, Varghese OK, et al. Enhanced photo electrochemical-response in highly ordered TiO_2 nanotube-arrays anodized in boric acid containing electrolyte. Sol Energy Mater Sol Cells 2006; 90 (9): 1283—95.

[93] Cai Q, Paulose M, Varghese OK, et al. The effect of electrolyte composition on the fabrication of self-organized titanium oxide nanotube arrays by anodic oxidation. J Mater Res 2005; 20(1): 230—6.

[94] Beranek R, Hildebrand H, Schmuki P. Self-organized porous titanium oxide prepared in H_2SO_4/HF electrolytes. Electrochem Solid-State Lett 2003; 6(3): B12—4.

[95] Macak JM, Sirotna K, Schmuki P. Self-organized porous titanium oxide prepared in Na_2SO_4/NaF electrolytes. Electrochim Acta 2005; 50(18): 3679－84.

[96] Shankar K, Mor GK, Prakasam HE, et al. Highly-ordered TiO_2 nanotube arrays up to 220 μm in length: use in water photoelectrolysis and dye-sensitized solar cells. Nanotech 2007; 18(1－11): 065707.

[97] Christophersen M, Carstensen J, Voigt K, et al. Organic and aqueous electrolytes used for etching macro—and mesoporous silicon. Phys Stat Sol A 2003; 197(1): 34－8.

[98] Taveira LV, Macák JM, Tsuchiya H, et al. Initiation and growth of self-organized TiO_2 nanotubes anodically formed in NH_4F/$(NH_4)_2SO_4$ electrolytes. J Electrochem Soc 2005; 152(10): B405－10.

[99] Wang J, Li HP, Stevens R. Hafnia and hafnia-toughened ceramics. J Mater Sci 1992; 27(20): 5397－430.

[100] Sundqvist J, Harsta A, Aarik J, et al. Atomic layer deposition of polycrystalline HfO_2 films by the HfI_4-O_2 precursor combination. Thin Solid Films 2003; 427(1－2): 147－51.

[101] Gilo M, Croitoru N. Study of HfO_2 films prepared by ion-assisted deposition using a gridless end-hall ion source. Thin Solid Films 1999; 350(1－2): 203－8.

[102] Waldorf AJ, Dobrowolski JA, Sullivan BT, et al. Optical coatings deposited by reactive ion plating. Appl Opt 1993; 32(28): 5583—93.

[103] Capone S, Leo G, Rella R, et al. Physical characterization of hafnium oxide thin films and their application as gas sensing devices. J Vac Sci Technol A 1998; 16(6): 3564－8.

[104] Esplandiu MJ, Avalle LB, Macagno VA. Characterization of hafnium oxide films modified by Pt doping. Electrochim Acta 1995; 40(16): 2587—93.

[105] Esplandiu MJ, Patrito EM, Macagno VA. Characterization of hafnium anodic oxide films: An AC impedance investigation. Electrochim Acta 1995; 40(7): 809—15.

[106] Ohtaki M, Peng J, Eguchi K, et al. Oxygen sensing properties of Ti-doped Nb_2O_5. Sens Actuat B 1993; (1－3): 495—6.

[107] Hutching GH, Taylor SH. Designing oxidation catalysts. Catal Today 1999; 49(1—3): 105－13.

[108] Aagard RI. Optical waveguide characteristics of reactive dc-sputtered niobium pentoxide films. Appl Phys Lett 1975; 27(11): 605—7.

[109] Ohtani B, Iwai K, Nishimoto S, et al. Electrochromism of niobium oxide thin films prepared by the sol-gel process. J Electrochem Soc 1994; 141(9): 2439—42.

[110] D'alkaine CV, De Souza LMM, Nart FC. The anodic behaviour of niobium—I. The state of the art. Corros Sci 1993; 34 (1): 109—15.

[111] Young L. Anodic Oxide Films. Academic Press, London, 1961.

[112] Karlinsey RL. Preparation of self-organized niobium oxide microstructures via potentiostatic anodization. Electrochem Commun 2005; 7(12): 1190—4.

[113] Choi J, Lim JH, Lee J, et al. Porous niobium oxide films prepared by anodization-annealing-anodization. Nanotech 2007; 18(5): 055603.

[114] Zhao JL, Wang XX, Xu RQ, et al. Preparation and growth mechanism of niobium oxide microcones by the anodization method. Electrochem Solid-State Lett 2007; 10(4): C31—3.

[115] Masuda Y, Wakamatsu S, Koumoto K. Site-selective deposition and micropatterning of tantalum oxide thin films using a monolayer. J Eur Ceram Soc 2004; 24(2): 301—7.

[116] Kamada K, Mukai M, Matsumoto Y. Anodic dissolution of tantalum and niobium in acetone solvent with halogen additives for electrochemical synthesis of Ta_2O_5 and Nb_2O_5 thin films. Electrochim Acta 2004; 49(2): 321—7.

[117] Mozalev A, Sakairi M, Saeki I, et al. Nucleation and growth of the nanostructured anodic oxides on tantalum and niobium under the porous alumina film. Electrochim Acta 2003; 48 (20—22): 3155—70.

[118] Vorobyova AI, Outkina EA. Thin Solid Films 1998; 324(1—2): 1—10.

[119] Kim WS, Kim JH, Kim JH, et al. Microwave dielectric properties of the ZrO_2-ZnO-Ta_2O_5-TiO_2 systems. Mater Chem Phys 2003; 79(2—3): 204—7.

[120] Vermilea DA. Ionic conductivity of anodic films at high field strengths: transient behavior. J Electrochem Soc 1957; 104 (7): 427—33.

[121] Sieber IV, Schmuki P. Porous tantalum oxide prepared by electrochemical anodic oxidation. J Electrochem Soc 2005; 152 (9): C639—44.

[122] Kawasaki H, Namba J, Iwatsuji K, et al. NO, gas sensing properties of tungsten oxide thin films synthesized by pulsed laser deposition method. Appl Surf Sci 2002; 197—198: 547—51.

[123] Gopel W, Schierbaum D. SnO_2 sensors-current status and future-prospects. Sens Actuat B 1995; 26(1—3): 1—12.

[124] Badilescu S, Ashrit PV. Study of sol-gel prepared nanostructured WO_3 thin films and composites for electrochromic applications. Solid State Ionics 2003; 158(1—2): 187—97.

[125] Ozkan E, Lee SH, Liu P, et al. Electrochromic and optical properties of mesoporous tungsten oxide films. Solid State Ionics 2002; 149(1—2): 139—46.

[126] Aliev AE, Shin HW. Nanostructured materials for electrochromic devices. Solid State Ionics 2002; (154—155): 425—31.

[127] Antonaia A, Addonizio ML, Minarini C, et al. Improvement in electrochromic response for an amorphous/crystalline WO_3 double layer. Electrochim Acta 2001; 46(13—14): 2221—7.

[128] Granqvist CG. Progress in electrochromics: tungsten oxide revisited. Electrochim Acta 1999; 44(18): 3005—15.

[129] Rauh RD. Electrochromic windows: an overview. Electrochim Acta 1999; 44(18): 3165—76.

[130] Lee SH, Cheong HM, Zhang JG, et al. Electrochromic mechanism in a-WO_{3-y} thin films. Appl Phys Lett 1999; 74 (2): 242—4.

[131] Sun M, Xu N, Cao YW, et al. Nanocrystalline tungsten oxide thin film: Preparation, microstructure, and photochromic behavior. J Mater Res 2000; 15(4): 927—33.

[134] Gavrilyuk AI. Photochromism in WO_3 thin films. Electrochim Acta 1999; 44(18): 3027—37.

[135] Di Quarto F, Di Paola A, Sunseri C. Semiconducting properties of anodic WO_3 amorphous films. Electrochim Acta 1981; 26(8): 1177—84.

[136] Beckstead DJ, Pepin GM, Ord JL. An optical study of hydrogen insertion in the anodic oxide of tungsten. J Electrochem Soc 1989; 136(2): 362—8.

[137] Ord JL, De Smet DJ. Anodic oxidation of tungsten in non-Aqueous electrolyte. J Electrochem Soc 1992; 139 (2): 359—63.

[138] Tsuchiya H, Macak JM, Sieber I, et al. Self-organized porous WO_3 formed in NaF electrolytes. Electrochem Commun 2005; 7(3): 295—8.

[139] Berger S, Tsuchiya H, Ghicov A, et al. High photocurrent conversion efficiency in self-organized porous WO_3.. Appl Phys Lett 2006; 88(20): 203119.

[140] De Tacconi NR, Chenthamarakshan CR, Yogeeswaran G., et al. Nanoporous TiO_2 and WO_3 films by anodization of titanium and tungsten substrates: influence of process variables on morphology and photoelectrochemical response. J Phys Chem B 2006; 110(50): 25347—55.

[141] Keil RG, Solomon RE. Anodization of vanadium in acetic acid solutions. J Electrochem Soc 1968; 115(6): 628—33.

[142] Keil RG, Solomon RE. Anodic oxide films on vanadium. J Electrochem Soc 1965; 112(6): 643—4.

[143] Ellis BH, Hopper MA, De Smet DJ. A study of the anodic oxidation of vanadium. J Electrochem Soc 1971; 118(6): 860—4.

[144] Ord JL, Bishop SD, DeSmet DJ. An optical study of hydrogen insertion in the anodic oxide of vanadium. J Electrochem Soc 1991; 138(1): 208—14.

[145] Arora MR, Kelly R. Some aspects of anodic-oxidation of V, Mo, and W. J Mater Sci 1977; 12(8): 1673—84.

[146] Arora MR, Kelly R. On the anodic sectioning of vanadium. J Electrochem Soc 1973; 120(1): 128—33.

[147] Mackintosh WD, Plattner HH. The anodic oxidation of vanadium: transport numbers of metal and oxygen and the metal/oxygen ratio in the oxide films. J Electrochem Soc 1976; 123 (4): 523—7.

[148] Chudnovskii FA, Stefanovich GB. Metal-insulator-transition in disordered VO_2.. J Solid State Chem 1992; 98(1): 137-43.

[149] Lewis MB, Perkins RA. The source of oxygen in the anodization of vanadium. J Electrochem Soc 1979; 126(4): 544-7.

[150] Hornkjøl S, Hornkjøl IM. Anodic behaviour of vanadium in acid solutions. Electrochim Acta 1991; 36(3-4): 577-80.

[151] Al-Kharafi FM, Badawy WA. Electrochemical behaviour of vanadium in aqueous solutions of different pH. Electrochim Acta 1997; 42(4): 579-86.

[152] Schreckenbach JP, Witke K, Butte D, et al. Characterization of thin metastable vanadium oxide films by Raman spectroscopy. Fresenius J Anal Chem 1999; 363(2): 211-4.

[153] Yamaguchi T. Application of ZrO_2 as a catalyst and a catalyst support. Catal Today 1994; 20(2): 199-217.

[154] Tanabe K, Yamaguchi T. Acid-base bifunctional catalysis by ZrO_2 and its mixed oxides. Catal Today 1994; 20(2): 185-97.

[155] Cox B. Factors affecting the growth of porous anodic oxide films on zirconium. J Electrochem Soc 1970; 117(5): 654-63.

[156] Ploc RA., Miller MA. Transmission and scanning electron microscopy of oxides anodically formed on zircaloy-2. J Nucl Mater 1977; 64(1-2): 71-85.

[157] Tsuchiya H, Schmuki P. Thick self-organized porous zirconium oxide formed in H_2SO_4/NH_4F electrolytes. Electrochem Commun 2004; 6(11): 1131-4.

[158] Spooner RC. Nature 1956; 178(4542): 1113-4.

[159] Hinde RS, Kellet EA, Harris PH. Sealing of aluminium oxide anodic films. Nature 1959; 183(4653): 39.

[160] Hart RK. A study of boehmite formation on aluminium surfaces by electron diffraction. Trans Faraday Soc 1954; 50: 269-73.

[161] Hunter MS, Towner PF, Robinson DL. Hydration of anodic oxide films. Proc Amer Electroplaters Soc 46th Ann Conf 1959; 3: 220.

[162] Bernard WJ, Randall Jr JJ. The reaction between anodic aluminum oxide and water. J Electrochem Soc 1961; 108(9): 822-5.

[163] Bengough GD, Stuart JM. Brit Patent 223995, 1925.

[164] Giles CH, Mehta HV, Stewart CE, et al. Adsorption at in organic surfaces. Part I. An investigation into the mechanism of adsorption of organic compounds by the anodic film on aluminium. J Chem Soc 1954: 4360—74.

[165] Schenk BM. Werkstoff aluminium und seine anodische oxidation. Verlag A. Francke, Berne, 1948.

[166] Hoar TP, Wood GC. The sealing of porous anodic oxide films on aluminium. Electrochim Acta 1962; 7(3): 333-53.

[167] Shingubara S. Fabrication of nanomaterials using porous alumina templates. J Nanoparticle Res 2003; 5(1-2): 17-30.

[168] Kokonou M, Rebholz C, Giannakopoulos KP, et al. Low aspect-ratio porous alumina templates. Microelectronic Eng 2008; 85(5-6): 1186-8.

[169] Sung SL, Tsai SH, Tseng CH, et al. Well-aligned carbon nitride nanotubes synthesized in anodic alumina by electron cyclotron resonance chemical vapor deposition. Appl Phys Lett 1999; 74(2): 197-9.

[170] Sun M, Zangari G, Shamsuzzoha M, et al. Electrodeposition of highly uniform magnetic nanoparticle arrays in ordered alumite. Appl Phys Lett 2001; 78(19): 2964-6.

[171] Su ZX, Sha J, Pan GW, et al. Temperature-dependent Raman scattering of silicon nanowires. J Phys Chem B 2006; 110(3): 1229-34.

[172] Asada T. Jpn Patent. 824505, 1969.

[173] Kawai S, Ishiguro I. Magnetic properties of anodic oxide coatings on aluminum containing electrodeposited Co and Co-Ni. J Electrochem Soc 1975; 122(1): 32-6.

[174] Kawai S, Ishiguro I. Recording characteristics of anodic oxide films on aluminum containing electrodeposited ferromagnetic metals and alloys. J Electrochem Soc 1976; 123(7): 1047-51.

[175] Sauer G, Brehm G, Schneider S, et al. Highly ordered monocrystalline silver nanowire arrays. J Appl Phys 2002; 91(5): 3243-7.

[176] Shingubara S, Okino O, Sakaue H, et al. Ordered two-dimensional nanowire array formation using self-organized nanoholes of anodically oxidized aluminum. Jpn J Appl Phys 1997; 36(12B): 7791-5.

[177] Sha J, Niu JJ, Ma XY, et al. Silicon nanotubes. Adv Mater 2002; 14(17): 1219-21.

[178] Varghese OK, Yang XP, Kendig J, et al. A transcutaneous hydrogen sensor: from design to application. Sensor Lett 2006; 4(2): 120-8.

(11 December 2008; accepted 30 December 2008)